

Structural, electrical and optical properties of copper-doped zinc oxide films deposited by spray pyrolysis

(Propriedades estruturais, elétricas e óticas de filmes de óxido de zinco dopados com cobre depositados por spray-pirólise)

J. S. C. Licurgo^{1*}, G. R. de Almeida Neto², H. R. Paes Junior¹

¹Universidade Estadual do Norte Fluminense Darcy Ribeiro, Advanced Materials Laboratory, Av. Alberto Lamego 2000, 28013-602, Campos dos Goytacazes, RJ, Brazil

²Federal University of São Carlos, Graduate Program in Materials Science and Engineering, S. Carlos, SP, Brazil

Abstract

The effect of copper doping on structural, electrical, and optical properties of zinc oxide films was evaluated. Copper-doped films (ZnO:Cu) were successfully deposited on a glass substrate by spray pyrolysis at doping levels of 0, 2.5, and 7.5 at% (ZnO, ZC2.5, ZC7.5). All films were polycrystalline, single-phase with ZnO hexagonal wurtzite structure. The films presented nanostructured crystallites, from 36.7 to 38.2 nm. Cu doping increased the electrical conductivity of the ZnO films; this change was proportional to the Cu concentration. The films presented high optical transmittance of 70-80% in the visible wavelength. The energy gap decreased upon Cu doping. The photoluminescence spectrum of all films displayed an intense ultraviolet emission and a weaker blue emission. The emissions shifted to lower wavelengths with increasing dopant concentrations. ZC7.5 presented the most promising properties for an application as transparent conducting oxide: intense optical transmittance and UV photoluminescence, also the lowest electrical resistivity.

Keywords: copper-doped zinc oxide films, spray pyrolysis, luminescence, transparent conducting oxide.

Resumo

O efeito da dopagem com cobre nas propriedades estruturais, elétricas e óticas de filmes de óxido de zinco foi avaliado. Filmes dopados com cobre (ZnO:Cu) foram depositados com sucesso em um substrato de vidro por spray-pirólise com concentração de dopante de 0, 2,5 e 7,5 %at (ZnO, ZC2.5, ZC7.5). Todos os filmes foram policristalinos, com fase wurtzita hexagonal do ZnO. Os filmes apresentaram cristaltitos nanoestruturados de 36,7 a 38,2 nm. A dopagem de cobre aumentou a condutividade elétrica dos filmes de ZnO; essa mudança foi proporcional ao teor de dopante. Os filmes apresentaram elevada transmitância ótica de 70-80% na região do espectro de luz visível. O gap ótico decresceu com a dopagem com Cu. Para todos os filmes o espectro de fotoluminescência apresentou emissão ultravioleta intensa e uma emissão azul mais fraca. As emissões se deslocaram para menores comprimentos de onda para maiores concentrações de dopante. ZC7.5 apresentou as propriedades mais promissoras para aplicações como óxido condutor transparente: transmitância ótica e fotoluminescência UV intensas, além da menor resistividade elétrica.

Palavras-chave: filmes de óxido de zinco dopados com cobre, spray-pirólise, luminescência, óxido condutor transparente.

INTRODUCTION

The progress of nanotechnology and nanoelectronics has attracted great interest in optoelectronic devices with multifunctional capacities. The increasing demand for low-cost and high-performance optoelectronic devices motivated the development of thin films of transparent conducting oxide (TCO). Since the first report regarding transparent oxide semiconductors by Bädeker in 1907 [1], the technological interest and value of these films have grown greatly. From this point on, deposition techniques

have been developed, and several electronic, optoelectronic, and mechanical applications have emerged. It is crucial that a TCO presents the lowest possible electrical resistivity and high optical transmittance (higher than 80%) in the visible region [2]. Tin-doped indium oxide (ITO) is the TCO that has been widely used in the industry due to its excellent electrical and optical properties. However, indium is toxic, expensive, and scarce [3]. Other materials have been studied to replace ITO in this expanding market. Zinc oxide (ZnO) is a candidate that has been receiving increasing attention.

ZnO is an II-IV semiconductor that has a high optical gap (3.3 eV), excellent chemical and thermal stability, high excitation energy, intense luminescence at room temperature, non-toxicity, wide availability, and low-cost.

*julianasclurgo@gmail.com

<https://orcid.org/0000-0002-8238-5842>

This combination of favorable properties makes it a potential candidate for applications in optoelectronic devices, ultrasonic transducers, gas sensors, solar cells, and others [4-9]. The doping of ZnO is a form to enhance some of its properties. Transition metals such as Mn [8], Cu [8, 10-17], Ag [18], Al [19], Co [20], Ni [21], Ti [22], and V [23] have been explored as dopants for ZnO. Copper is especially interesting due to similar ionic radius and electronic structure to Zn, in addition to behaving as a luminescence activator through the creation of energy levels in the ZnO forbidden bands [8, 17, 24]. Mani and Rayappan [25] found superior NH₃ sensing properties for Cu-doped ZnO. Similarly, Shewale *et al.* [24] found that 4 wt% of Cu present the optimal performance for H₂S sensing. Liu *et al.* [26] studied nanopowders of Cu-doped ZnO and observed intrinsic ferromagnetism at room temperature. Singhal *et al.* [27] found the solubility limit of Cu in ZnO to be 10 at% and observed DC electrical resistivity and activation energy decreasing with copper doping levels. Licurgo and Paes Junior [10] observed a decrease in band gap value with Cu doping.

Cu-doped ZnO films can be produced by a great variety of deposition methods, as DC and RF magnetron sputtering [28], ice-bath assisted sonochemical method [11], sol-gel [29], sol-gel spin coating [30], pulsed laser deposition technique [31], and spray pyrolysis [10, 13]. Among the available techniques, spray pyrolysis is especially interesting since it is easily operated, low-cost, reproducible, and can be deposited on substrates with different geometries. In this paper, nanocrystalline thin films of ZnO and Cu-doped ZnO were prepared on a glass substrate by spray pyrolysis technique. The films were comprehensively characterized in order to understand the effect of copper doping on ZnO properties. The morphological, structural, and electrical characterization were combined with the study of the optical absorption and photoluminescence behavior, providing valuable information on the doping process through this simple and cheap technique.

MATERIALS AND METHODS

Film deposition: ZnO film was prepared using the methodology described in the previous work of our research group [10]. Briefly, a precursor solution was prepared for the deposition of the ZnO films. A solution of 0.1 M zinc acetate [Zn(CH₃COO)₂·2H₂O, ACS grade, 98%, Sigma Aldrich] was diluted in deionized water and isopropyl alcohol (ACS grade, 99.5%, Isolar) in a 1:3 ratio (deionized water:alcohol). A solution of 0.02 M copper chloride (CuCl₂·2H₂O, ACS grade, 99%, Sigma Aldrich) diluted in deionized water was used for doping the films with copper. Then, approximately 1 mL of acetic acid was added to the solution in order to neutralize the solution pH. ZnO:Cu solutions were prepared to yield a Cu doping of 0, 2.5, and 7.5 at%, which were referred to as ZnO, ZC2.5, and ZC7.5, respectively. Spray pyrolysis was the technique used for the film deposition. This technique consists of the atomization of a precursor solution, composed of ions of interest, on a pre-heated substrate. The droplets, when in contact with the heated substrate, decompose and react to

form the desired chemical compounds. In this study, a home-made spray pyrolysis apparatus was used. The films were deposited for 30 min using a glass substrate temperature of 450 °C, compressed air pressure of 1.5 kgf/cm² and precursor solution flow rate of 1.5 mL/min.

Characterization of the films: morphological characterization of the films was performed in a laser confocal scanning microscope (Olympus, LEXT OLS 4000). The top surface micrographs were obtained for morphological analyses, and the film cross-section was analyzed in order to measure the film thickness. Structural characterization was performed by X-ray diffraction (XRD) technique in a diffractometer (Rigaku, Ultima IV). The following measurement parameters were used: CuK α radiation (wavelength of 1.54 Å), step size of 0.05°, scanning speed of 1 °.min⁻¹, counting time of 3 s, and scanning range from 20° to 80° (2 θ). The crystallite size was calculated using the Debye-Scherrer equation for the most intense peak:

$$D_{hkl} = K \cdot \frac{\lambda}{B_{hkl} \cdot \cos\theta_{hkl}} \quad (A)$$

where K is a constant that depends on the crystallite geometry (assumed as 0.9 for spherical crystallite), λ is the incident radiation wavelength (1.5406 Å), B_{hkl} is the full width at half maximum (FWHM), and θ is the Bragg's diffraction angle. The interplanar spacing d_{hkl} between (hkl) planes was calculated using Bragg's law [17]. The lattice parameters a and c of the films were calculated by [12]:

$$\frac{1}{d_{hkl}^2} = \frac{4}{3} \cdot \left(\frac{h^2 + h \cdot k + k^2}{a^2} \right) + \frac{1}{c^2} \quad (B)$$

Electrical characterization was carried out by measuring the electrical conductivity (σ) variation as a function of temperature (T). The two-point probe method was used to obtain the film conductivity in a multimeter (Agilent, 3458). The activation energy for the electrical conduction process was calculated by:

$$\beta = \frac{-E_a}{k} \quad (C)$$

where β is the slope of the $\ln\sigma$ vs. $T^{-1} \times 10^3$ curve, E_a (eV) is the activation energy, and k is the Boltzmann constant. Sheet resistance was measured at room temperature using a 4-point head (Cascade Microtech, C4S-44/5S) in a multimeter (Agilent, 3458) with a home-made current source. From the sheet resistance, the electrical resistivity was calculated by:

$$R_{sh} = \frac{\rho}{e} \quad (D)$$

where R_{sh} is the sheet resistance ($\Omega \cdot \square^{-1}$), and ρ is the electrical resistivity ($\Omega \cdot \text{cm}$). The variation of the film optical transmittance (T_0) as a function of the incident radiation wavelength (λ) was the method used for the optical

characterization of the films. The spectra were obtained using a spectrophotometer (Specord, M500) in the wavelength range from 300 to 850 nm. The absorption coefficient (α) was calculated using Eq. E [32]. The optical gap of the films was obtained by the extrapolation of the linear portion of the $(\alpha \cdot hv)^2$ vs. hv curve to the hv axis [32].

$$a = \frac{1}{e} \cdot \ln \frac{1}{T_0} \quad (E)$$

where α is the absorption coefficient, and T_0 is the optical transmittance. Photoluminescence measurements were performed in a spectrofluorophotometer (Shimadzu, RF-5301PC). In this technique, light with the desired wavelength is directed to the sample to obtain the emission spectrum. The measurements were performed at an excitation wavelength of 325 nm.

RESULTS AND DISCUSSION

Morphological characterization: most applications in the electronic and optoelectronics industry require films of high quality, with the lowest concentration of defects. The films produced in our study by spray pyrolysis were well-adhered to the glass substrate and homogeneous. In Fig. 1, the top surface micrographs of the films are shown. There were no cracks or other types of defects on the surfaces. Also, they presented nanoscale grains, and there was no clear morphology difference between the film surfaces.

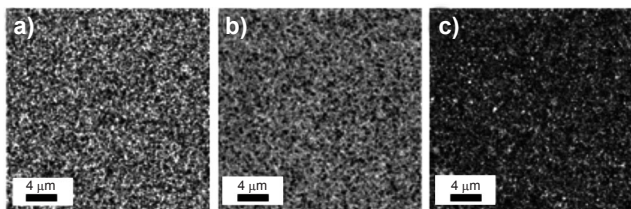


Figure 1: Laser confocal scanning microscope micrographs of the film top surfaces of: a) ZnO; b) ZC2.5; and c) ZC7.5.

[Figura 1: Micrografias de microscópio de varredura confocal a laser das superfícies superiores dos filmes: a) ZnO; b) ZC2.5; e c) ZC7.5.]

Structural characterization: XRD diffractograms of the films are presented in Fig. 2. The identified peaks of ZnO and Cu-doped ZnO matched the ZnO hexagonal wurtzite pattern (JCPDS #36-1451). The doping of ZnO with Cu did not modify its structure. Furthermore, diffraction peaks associated with CuO or other Cu compounds were not identified. These findings suggested that Cu ions occupy substitutional sites into ZnO hexagonal structure. The films presented similar relative peak intensities; the peak related to the (002) plane was the most intense for all films, followed by the (101) (Fig. 2). This revealed a preferential crystal growth along the c-axis (002), which is perpendicular to the substrate surface. The relative intensity of the (002) peak $[I_{002}/(I_{002}+I_{102}+I_{101})]$ was 0.6, 0.6 and 0.5, for ZnO, ZC2.5 and ZC7.5, respectively. In the literature, there is not a clear trend regarding the change of

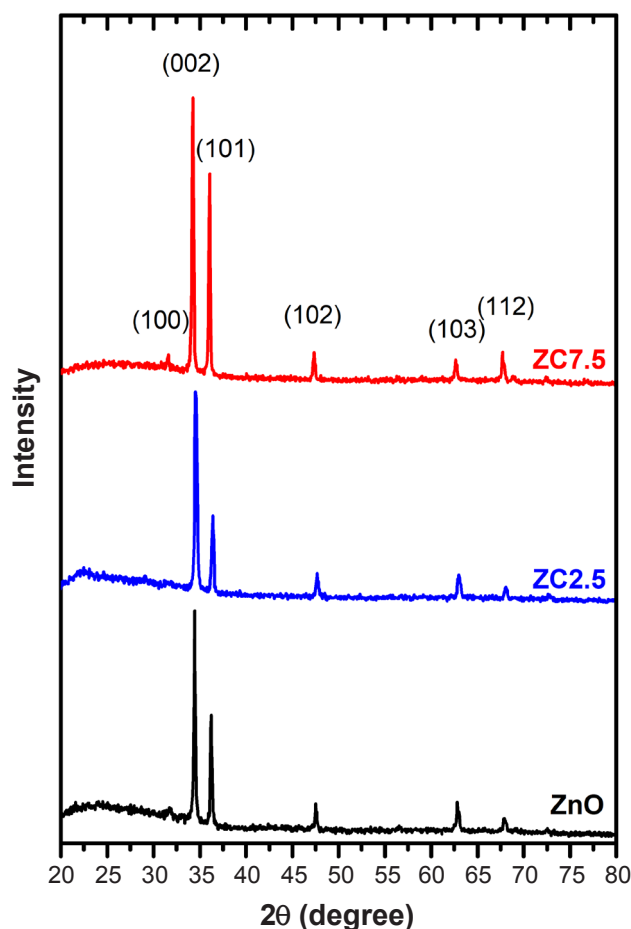


Figure 2: X-ray diffraction patterns of ZnO, ZC2.5, and ZC7.5 films.

[Figura 2: Difratoformas de raios X dos filmes ZnO, ZC2.5 e ZC7.5.]

ZnO (002) peak intensity upon Cu doping [8].

The calculated lattice parameters (a , c) and volume (V) were similar to the values of the JCPDS 36-1451 (Table I). It was observed that ZC2.5 displayed slightly smaller lattice parameters than intrinsic ZnO. However, for higher doping concentration (ZC7.5), it was observed that a and c increased, leading to an expanded unit cell volume. Othman *et al.* [11] observed similar behavior for Cu-doped ZnO films produced by the sonochemical method. The unit cell volume reduced for Cu concentration below 5 at%, and then a sudden increase for higher doping concentrations was observed. The doping process shifted the position of all ZnO diffraction peaks, shifting them to higher 2θ for 2.5 at% Cu, and to lower 2θ for 7.5 at% Cu. Regarding the most intense peak (002), the doping process shifted the peak position from a 2θ of 34.45° to 34.55° and 34.25° , for ZC2.5 and ZC7.5, respectively. The shift of the position of the peaks may be related to the incorporation of Cu into the ZnO structure. The ionic radii of Cu^{1+} , Cu^{2+} and Zn^{2+} are 0.096, 0.072 and 0.074 nm, respectively. Therefore, the valence state of the Cu ion that is doped into ZnO has an important role in the change of the c -axis (002). A higher diffraction angle relates to smaller interplanar spacing. Then, it is likely to believe

Table I - Properties obtained from XRD data of ZnO, ZC2.5, and ZC7.5 films.
 [Tabela I - Propriedades obtidas por dados do DRX dos filmes ZnO, ZC2.5 e ZC7.5.]

Sample	FWHM $\beta_{(002)}$	Crystallite size (nm)	a (Å)	c (Å)	c/a	V (Å ³)
ZnO	0.2238	37.1	3.25	5.21	1.60	47.74
ZC2.5	0.2971	36.7	3.24	5.19	1.60	47.16
ZC7.5	0.2178	38.2	3.27	5.24	1.60	48.49

that Cu doping leads to substitution of Zn²⁺ predominantly by Cu²⁺. Othman *et al.* [11] observed the same behavior, where the (002) peak position shifted to a higher angle for Cu concentration of 4 at%, and then it moved to a lower angle for 5 at%. The authors believe that this shift was caused by the distortion of ZnO lattice by the introduction of larger concentrations of Cu.

The crystallite size of the films was calculated by Scherrer formula using FWHM of ZnO (002) peak (Table I). All films presented a crystallite size smaller than 39 nm. The doping process did not significantly change the ZnO film crystallite size. Nimbalkar and Patil [12] also found a negligible change of crystallite size upon Cu doping. Rahmani *et al.* [13] and Tarwal *et al.* [14] studied spray pyrolyzed films of ZnO, and reported the crystallite size of 16-38 and 22-42 nm, respectively; these results agree with the obtained herein.

Electrical characterization: the influence of temperature on the electrical conductivity of the samples is presented in Fig. 3. A typical semiconductor behavior was observed for the films, where the electrical conductivity increased with temperature. The electrical conductivity of the intrinsic ZnO film was similar to that of ZnO nanorods, also obtained by spray pyrolysis [33]. Cu-doped samples presented higher electrical conductivity than that of intrinsic ZnO. The increase was more pronounced for higher doping concentration. This result agreed with those reported in other studies [12, 15, 27, 34, 35], and this increase was likely due to a higher concentration of free carriers [15]. Other authors [34] suggested that Cu may reduce ZnO, originating deficiency of oxygen, and producing nonstoichiometry in the sample. The activation energy for the electrical conduction process did not change significantly with Cu doping concentration (Table II).

The electrical resistivity of the films was obtained at room temperature by the 4-point probe method (Table II). The incorporation of the dopant was effective, decreasing the films' electrical resistivity. The incorporation of Cu into the ZnO host matrix occurred mainly in the +2 valence state by replacing Zn²⁺ sites, resulting in an increased concentration of free carriers, which was caused by the lower ionization potential of Cu atoms than that of Zn. In the doped films, the crystallite size slightly increased with the dopant concentration, which reduced the grain boundary scattering. These two behaviors provided an increment on the electrical conductivity of the doped films in comparison to the intrinsic film. Oxygen desorption performs an important role in the activation energy of the electrical

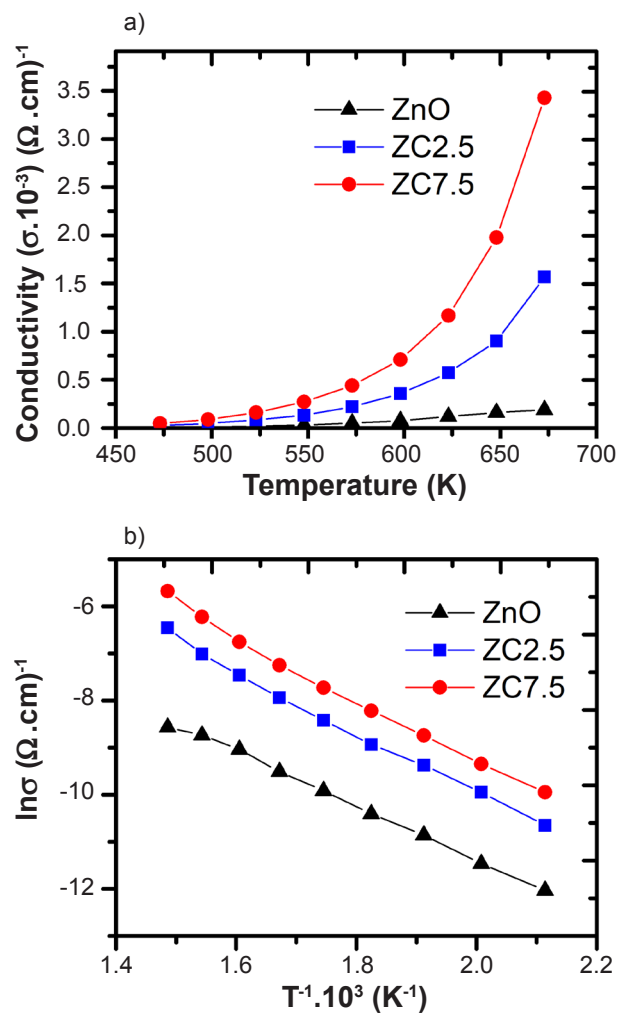


Figure 3: Curves of electrical conductivity as a function of temperature (a) and its natural logarithm as a function of the inverse of temperature (b) of ZnO, ZC2.5, and ZC7.5 films.

[Figura 3: Curvas de condutividade elétrica em função da temperatura (a) e seu logaritmo natural em função do inverso da temperatura (b) dos filmes ZnO, ZC2.5 e ZC7.5.]

conduction process, as suggested in [36], indicating the presence of deep donor levels, from which the carriers jump to the conduction band by a thermally activated process. The values of electrical resistivity obtained in this study were lower than the reported for DC and radio frequency (RF) magnetron sputtered films [16, 28, 37, 38]. This indicates that high-quality films can be obtained using a cheaper and simpler deposition technique, spray pyrolysis.

Table II - Properties obtained from the electrical and optical characterization of ZnO, ZC2.5, and ZC7.5 films.

[Tabela II - Propriedades obtidas por caracterizações elétricas e óticas dos filmes ZnO, ZC2.5 e ZC7.5.]

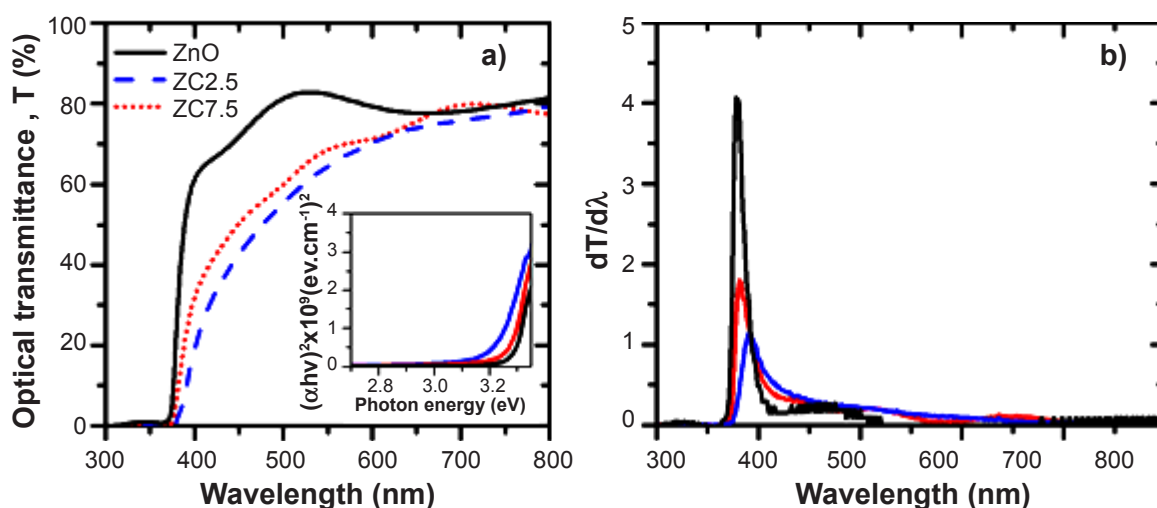
Sample	Activation energy (eV)	Resistivity (Ω .cm)	Absorption coefficient (cm^{-1})	Optical gap (eV)
ZnO	0.50	6.58	6.2×10^2	3.27
ZC2.5	0.53	5.84	9.2×10^2	3.18
ZC7.5	0.54	2.93	1.1×10^3	3.24

Optical characterization: the curves of optical transmittance of the ZnO:Cu films are presented in Fig. 4. The films displayed intense optical transmittance within the visible spectrum. High transmittance in a large range of wavelengths can be useful for a variety of optical applications [39]. Films with low electrical resistivity are likely to present high optical quality due to low dispersion or absorption losses. Intrinsic ZnO film presented sharper absorption edge and high optical transmittance of approximately 80% in the wavelength range of 380 to 800 nm (Fig. 4). The optical transmittance of ZC2.5 and ZC7.5 films were smaller than that of ZnO from 380 to nearly 650 nm. However, it still reached approximately 70% at a wavelength of 550 nm and continued to increase until ~80% at 800 nm. A high transmittance is an important property for TCO applications, and it reveals the films' morphological homogeneity and crystal quality [33]. However, the lower optical transmittance for ZC2.5 and ZC7.5 may be due to the increase of absorbing centers with the incorporation of Cu, consequently increasing the film light absorption capacity. Moreover, the decrease of transmittance can also be associated with the scattering of incident photons by the incorporation of copper at the substitutional or interstitial sites in the ZnO matrix. Similar results were found in [16, 17]. Tarwal *et al.* [14] observed a drop of transmittance to

nearly 70% at 600 nm for a doping concentration of 5 and 10 at% of Cu, which matches the values observed in our study. The authors observed that the doping of 20 at% of Cu decreases it, even more, reaching 50% of transmittance [14].

The optical gap and absorption coefficient of the films, which was calculated at the wavelength of 550 nm, are presented in Table II. Cu-doped films presented a greater absorption coefficient and a slightly smaller optical gap. The decrease in the optical gap can be explained by the optical gap of CuO (1.40 eV) being smaller than that of ZnO (3.37 eV) and the difference of Zn and Cu electronegativities [14, 40]. It has also been proposed that this reduction is due to the hybridization of 3d orbitals of Cu with 2p bands of O [41]. The trend found herein matches those of previously published studies [13, 14, 17, 25]. In order to study the absorption edge of the samples, the curves of the derivative of transmittance ($dT/d\lambda$) versus wavelength of the samples were plotted (Fig. 4b). It was observed that all samples presented a sharp absorption edge, presenting a peak related to the optical band gap, which intensity is directly related to the optical gap values [42]. The optical gap obtained by this method matches closely that of the Tauc plot.

The photoluminescence spectra of ZnO and Cu-doped ZnO films are presented in Fig. 5. ZnO film presented intense and weak UV emissions around 396 nm (3.13 eV)

Figure 4: Optical transmittance as a function of wavelength and the inset of $(\alpha \cdot hv)^2$ versus $h\nu$ (a), and the curves of the derivative of transmittance ($dT/d\lambda$) versus wavelength (b) of the ZnO, ZC2.5, and ZC7.5 films.[Figura 4: Transmittância ótica em função do comprimento de onda e inserto de $(\alpha \cdot hv)^2$ versus $h\nu$ (a) e curvas de derivada de transmittância ($dT/d\lambda$) versus comprimento de onda dos filmes ZnO, ZC2.5 e ZC7.5.]

and 361 nm (3.43 eV), respectively. This was related to the near-band edge (NBE) free exciton transition. Emission in the blue spectrum around 470 nm (2.64 eV) was also observed. It is likely that the blue emission is related to the recombination of trapped electrons at shallow bands of interstitial Zn with photo-generated holes [11, 43] and/or the decay from Zn interstitial level to Cu⁺ [29]. Spectra with similar characteristics were obtained in [40]. The photoluminescence intensity decreased upon Cu-doping, which indicated that a nonradiative recombination process, such as Auger, occurred in the samples [11]. Recombination centers tend to increase with higher doping concentration and structural defects [44]. Therefore, it is likely that the disappearance of the weaker NBE emission of the ZnO after Cu doping is due to the formation of Cu acceptor levels and the introduction of defect levels in the ZnO optical band gap, leading to increased nonradiative recombination processes [38]. Structural defects such as oxygen vacancies are known for increasing the green emission [16]; since there was no significant green emission, it is believed that the density of this defect was low [14]. With the incorporation of Cu in the ZnO matrix, all emission shifted to lower wavelengths; the shift was more expressive for increasing Cu content. The intense UV emission shifted to 395 nm (3.14 eV) and 391 nm (3.17 eV) for ZC2.5 and ZC7.5 films, respectively. Furthermore, the emission peaks of Cu-doped films were broader than the peaks of intrinsic film.

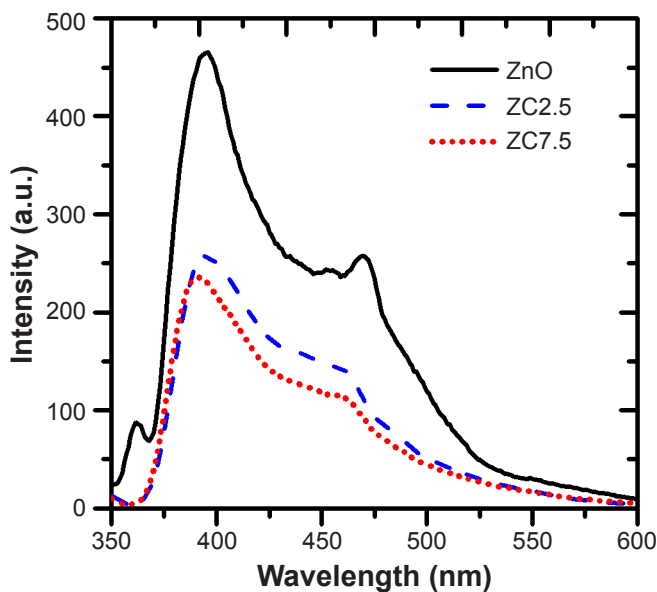


Figure 5: Photoluminescence spectrum of the ZnO, ZC2.5, and ZC7.5 films.

[Figura 5: Espectro de fotoluminescência dos filmes ZnO, ZC2.5 e ZC7.5.]

CONCLUSIONS

Thin films were successfully prepared by the spray pyrolysis technique. The doping of ZnO with Cu changed the properties of the films significantly. On the XRD

patterns, diffraction peaks related to CuO or other Cu compounds were not identified; all samples presented only the ZnO hexagonal wurtzite structure. This indicated that the doping was effective, where the Cu atoms occupied the substitutional sites of Zn. The predominant valence state of Cu seemed to be Cu²⁺. The film crystallite size was not significantly affected by the doping process, ranging from 36.7 to 38.2 nm. ZnO presented a typical semiconductor behavior, where electrical conductivity increased with temperature. The doping of Cu was beneficial for electrical conductivity. The Cu-doped ZnO films presented higher electrical conductivity than that of ZnO, and higher doping levels led to higher electrical conductivity. The optical transmittance results were satisfactory for the application as TCO (transparent conducting oxide), presenting intense transmittance of nearly 70-80% in the visible wavelength. Regarding the photoluminescence spectra, the films presented similar behavior, intense UV emission between 391 and 396 nm, and weaker blue emission between 460 and 470 nm. The results of this investigation showed that ZC7.5 (ZnO 7.5 at% Cu) was the film that presented the most appropriate properties for TCO applications, combining higher electrical conductivity with desired photoluminescence spectrum and intense optical transmittance in the visible wavelength range.

ACKNOWLEDGMENTS

This study was financed in part by the Coordenação de Aperfeiçoamento de Pessoal de Nível Superior - Brasil (CAPES) - Finance Code 001. The authors would like to thank CNPq for J.S.C. Licurgo Masters Scholarship.

REFERENCES

- [1] K. Bädeker, *Ann. Phys.* **327**, 4 (1907) 749.
- [2] B.G. Lewis, D.C. Paine, *MRS Bull.* **25**, 8 (2000) 22.
- [3] T. Minami, *Semicond. Sci. Technol.* **20**, 4 (2005) S35.
- [4] Y. Wang, M. Xu, J. Li, J. Ma, X. Wang, Z. Wei, X. Chu, X. Fang, F. Jin, *Surf. Coat. Technol.* **330** (2017) 255.
- [5] X.S. Zhou, C. Zhao, R. Hou, J. Zhang, K.J. Kirk, D. Hutson, Y.J. Guo, P.A. Hu, S.M. Peng, X.T. Zu, Y.Q. Fu, *Ultrasonics* **54**, 7 (2014) 1991.
- [6] L. Zhu, W. Zeng, *Sens. Actuator A Phys.* **267** (2017) 242.
- [7] Z. Mo, Y. Huang, S. Lu, Y. Fu, X. Shen, H. He, *Optik* **149** (2017) 63.
- [8] Z. Banu Bahşi, A.Y. Oral, *Opt. Mater.* **29**, 6 (2007) 672.
- [9] Ü. Özgür, Y.I. Alivov, C. Liu, A. Teke, M.A. Reshchikov, S. Doğan, V. Avrutin, S.-J. Cho, H. Morkoç, *J. Appl. Phys.* **98**, 4 (2005) 41301.
- [10] J.S.C. Licurgo, H.R. Paes Junior, *Mater. Sci. Forum* **930** (2018) 79.
- [11] A.A. Othman, M.A. Ali, E.M.M. Ibrahim, M.A. Osman, *J. Alloys Compd.* **683** (2016) 399.
- [12] A.R. Nimbalkar, M.G. Patil, *Mater. Sci. Semicond. Process.* **71** (2017) 332.
- [13] M.B. Rahmani, S.H. Keshmiri, M. Shafiei, K. Latham, W. Wlodarski, J. du Plessis, K. Kalantar-Zadeh, *Sens. Lett.*

- 7, 4 (2009) 621.
- [14] N.L.L. Tarwal, K.V.V. Gurav, S.H.H. Mujawar, S.B.B. Sadale, K.W.W. Nam, W.R.R. Bae, A.V.V. Moholkar, J.H.H. Kim, P.S.S. Patil, J.H.H. Jang, *Ceram. Int.* **40**, 6 (2014) 7669.
- [15] K. Omri, A. Bettaibi, K. Khirouni, L. El Mir, *Phys. B Condens. Matter* **537** (2018) 167.
- [16] A. Sreedhar, J.H. Kwon, J. Yi, J.S. Kim, J.S. Gwag, *Mater. Sci. Semicond. Process.* **49** (2016) 8.
- [17] A. Mhamdi, R. Mimouni, A. Amlouk, M. Amlouk, S. Belgacem, *J. Alloys Compd.* **610** (2014) 250.
- [18] L. Duan, B. Lin, W. Zhang, S. Zhong, Z. Fu, *Appl. Phys. Lett.* **88**, 23 (2006) 232110.
- [19] P.P. Sahay, R.K. Nath, *Sens. Actuators B Chem.* **134**, 2 (2008) 654.
- [20] J. Hyun Kim, H. Kim, D. Kim, Y. Ihm, W. Kil Choo, *J. Eur. Ceram. Soc.* **24**, 6 (2004) 1847.
- [21] J.H. He, C.S. Lao, L.J. Chen, D. Davidovic, Z.L. Wang, *J. Am. Chem. Soc.* **127**, 47 (2005) 16376.
- [22] S.-S. Lin, J.-L. Huang, P. Šajgalik, *Surf. Coat. Technol.* **191**, 2-3 (2005) 286.
- [23] H. Saeki, H. Tabata, T. Kawai, *Solid State Commun.* **120**, 11 (2001) 439.
- [24] P.S. Shewale, V.B. Patil, S.W. Shin, J.H. Kim, M.D. Uplane, *Sens. Actuators B Chem.* **186** (2013) 226.
- [25] G.K. Mani, J.B.B. Rayappan, *J. Alloys Compd.* **582** (2014) 414.
- [26] H.L. Liu, J.H. Yang, Y.J. Zhang, Y.X. Wang, M.B. Wei, D.D. Wang, L.Y. Zhao, J.H. Lang, M. Gao, *J. Mater. Sci. Mater. Electron.* **20**, 7 (2009) 628.
- [27] S. Singhal, J. Kaur, T. Namgyal, R. Sharma, *Physica B Condens. Matter* **407**, 8 (2012) 1223.
- [28] D.R. Sahu, *Mater. Sci. Eng. B* **171**, 1-3 (2010) 99.
- [29] L. Xu, F. Xian, G. Zheng, M. Lai, *Mater. Res. Bull.* **99** (2018) 144.
- [30] K.R. Gbashi, A.T. Salih, A.A. Najim, M.A.H. Muhi, *J. Mater. Sci. Mater. Electron.* **28**, 20 (2017) 15089.
- [31] Q.A. Drmash, S.G. Rao, Z.H. Yamani, M.A. Gondal, *Appl. Surf. Sci.* **270** (2013) 104.
- [32] J.I. Pankove, *Optical processes in semiconductors*, Dover Publ., New York (1971).
- [33] E. Karaköse, H. Çolak, *Energy* **140** (2017) 92.
- [34] H. Çolak, O. Türkoğlu, *Mater. High Temp.* **29**, 4 (2012) 344.
- [35] Y.S. Sonawane, K.G. Kanade, B.B. Kale, R.C. Aiyer, *Mater. Res. Bull.* **43**, 10 (2008) 2719.
- [36] S. Fujitsu, K. Koumoto, H. Yanagida, Y. Watanabe, H. Kawazoe, *Jpn. J. Appl. Phys.* **38**, 1 3A (1999) 1534.
- [37] M. Imran, R. Ahmad, N. Afzal, M. Rafique, *Vacuum* **165** (2019) 72.
- [38] A.C. Saritha, M.R. Shijeesh, L.S. Vikas, R.R. Prabhu, M.K. Jayaraj, *J. Phys. D Appl. Phys.* **49**, 29 (2016) 295105.
- [39] V. Ganesh, I.S. Yahia, S. AlFaify, M. Shkir, *J. Phys. Chem. Solids* **100** (2017) 115.
- [40] F. Jamali-Sheini, R. Yousefi, *Ceram. Int.* **39**, 4 (2013) 3715.
- [41] M. Ferhat, A. Zaoui, R. Ahuja, *Appl. Phys. Lett.* **94**, 14 (2009) 142502.
- [42] I.S. Yahia, A.A.M. Farag, M. Cavas, F. Yakuphanoglu, *Superlattices Microstruct.* **53** (2013) 63.
- [43] H. Zeng, G. Duan, Y. Li, S. Yang, X. Xu, W. Cai, *Adv. Funct. Mater.* **20**, 4 (2010) 561.
- [44] Z.F. Liu, F.K. Shan, J.Y. Sohn, S.C. Kim, G.Y. Kim, Y.X. Li, J.Y. Sohn, *J. Electroceramics* **13**, 1-3 (2004) 183.
- (*Rec.* 22/10/2019, *Rev.* 06/02/2020, 16/03/2020, *Ac.* 20/03/2020)